Biophysical *Journal*
Article

Biophysical Society

Optical Recording of Action Potential Initiation and Propagation in Mouse Skeletal Muscle Fibers

Quinton Banks,[1] Stephen Joseph Paul Pratt,[1] Shama Rajan Iyer,[2] Richard Michael Lovering,[2] Erick Omar Hernández-Ochoa,[1] and Martin Frederick Schneider[1,*]
[1]Department of Biochemistry and Molecular Biology and [2]Department of Orthopedics, University of Maryland School of Medicine, Baltimore, Maryland

ABSTRACT Skeletal muscle fibers have been used to examine a variety of cellular functions and pathologies. Among other parameters, skeletal muscle action potential (AP) propagation has been measured to assess the integrity and function of skeletal muscle. In this work, we utilize 1-(3-sulfonatopropyl)-4[β[2-(Di-*n*-octylamino)-6-naphtyl]vinyl]pyridinium betaine, a potentiometric dye, and mag-fluo-4, a low-affinity intracellular Ca^{2+}indicator, to noninvasively and reliably measure AP conduction velocity in skeletal muscle. We used remote extracellular bipolar electrodes to generate an alternating polarity electric field that initiates an AP at either end of the fiber. Using enzymatically dissociated flexor digitorum brevis (FDB) fibers and high-speed line scans, we determine the conduction velocity to be ~0.4 m/s. We applied these methodologies to FDB fibers under elevated extracellular potassium conditions and confirmed that the conduction velocity is significantly reduced in elevated $[K^+]_o$. Because our recorded velocities for FDB fibers were much slower than previously reported for other muscle groups, we compared the conduction velocity in FDB fibers to that of extensor digitorum longus (EDL) fibers and measured a significantly faster velocity in EDL fibers than FDB fibers. As a basis for this difference in conduction velocity, we found a similarly higher level of expression of Na^+ channels in EDL than in FDB fibers. In addition to measuring the conduction velocity, we can also measure the passive electrotonic potentials elicited by pulses by applying tetrodotoxin and have constructed a circuit model of a skeletal muscle fiber to predict passive polarization of the fiber by the field stimuli. Our predictions from the model fiber closely resemble the recordings acquired from in vitro assays. With these techniques, we can examine how various pathologies and mutations affect skeletal muscle AP propagation. Our work demonstrates the utility of using 1-(3-sulfonatopropyl)-4[β[2-(Di-*n*-octylamino)-6-naphtyl]vinyl]pyridinium betaine or mag-fluo-4 to noninvasively measure AP initiation and conduction.

INTRODUCTION

The action potential (AP) conduction velocity is a basic biophysical property of long excitable cells and neurons. In nerve axons, the AP conduction velocity determines the timing of information transfer from point to point in the nervous system. In skeletal muscle fibers, the AP is initiated at the neuromuscular junction, roughly in the middle of the fiber, and propagates longitudinally and radially toward both ends of the fiber via the surface sarcolemma and the t-tubule (TT) system (1). The AP conduction velocity, together with the fiber length, then determines the degree of synchrony of the arrival of the AP and consequently the synchrony of contractile activation along the muscle fiber (2). This is important because asynchronous contractile activation would result in ineffective local force generation and/or inappropriate local shortening by the muscle fiber. In chronic or extreme cases, this could reduce whole-muscle function and likely cause muscle damage. Conduction velocity, and thus synchrony, could itself be affected by disruption or dysregulation of the membrane (3), dysfunction of ion channels, and other proteins responsible for the AP initiation and propagation (4), among numerous possibilities. Indeed, alterations in the AP conduction properties have been described in disease conditions (5–9). Therefore, investigating the conduction velocity of skeletal muscle fiber APs is an important functional parameter in muscle biophysics.

Traditional studies have examined skeletal muscle AP conduction velocity using intracellular microelectrode techniques or electromyography in human and animal models (10–12). Although these methods have allowed us to understand many different aspects of muscle physiology, they have their limitations. Microelectrode impalement or patch-clamp pipettes in the whole-cell configuration can be damaging, likely via disruption of the sarcolemma and

Submitted March 23, 2018, and accepted for publication October 24, 2018.
*Correspondence: mschneider@som.umaryland.edu
Editor: Eric Sobie.
https://doi.org/10.1016/j.bpj.2018.10.026

intracellular milieu. Electromyography records from gross muscle are ideal for the study of muscle fiber groups but not for studies in in individual cells.

The use of noninvasive optical methods to measure skeletal muscle AP was introduced by Vergara and Bezanilla to demonstrate the existence of the "t-tubule AP" (13). Recent studies have utilized newer potentiometric dyes and calcium (Ca^{2+}) indicators to the measure AP and AP-induced Ca^{2+} transients of muscle at the single-cell level (14–17). Edwards and colleagues used Ca^{2+} indicators to measure AP conduction velocity in the transverse and longitudinal tubule systems of mechanically skinned fibers after mechanical removal of the sarcolemma (15). Recently, 1-(3-sulfonatopropyl)-4[β [2-(Di-*n*-octylamino)-6-naphtyl]vinyl]pyridinium betaine (di-8-ANEPPS), a voltage-sensitive dye, was used to measure the AP simultaneously at multiple locations along the TT system and to resolve the radial AP propagation (14). Both sarcolemmal and TT AP conduction are required for synchronic activation of the muscle contraction; however, AP conduction velocity either radially or longitudinally within the TT network has been studied in relatively more detail, whereas the properties of the surface sarcolemmal AP conduction in intact muscle fibers have remained less explored.

Here, we take advantage of the ability to initiate an AP at one end of the fiber or the other end by simply varying the polarity of electric field stimulation via remote bipolar electrodes (18). Using this approach, we have refined and validated a new method, to our knowledge, to noninvasively measure the conduction velocity of the AP along the sarcolemma in isolated skeletal muscle fibers and whole muscle. To our knowledge, this is the first report of using recording at a single spatial location (near the end of a muscle fiber) together with alternating-polarity electric field stimulation to determine surface AP conduction velocity. Traditionally, the AP conduction velocity has been measured experimentally by electrically stimulating a nerve or muscle and monitoring the arrival of the AP at two different spatial locations as the AP propagates along a fiber.

Using this new, to our knowledge, method, we were able to identify that the conduction velocity is greater in long EDL muscle fibers than in the shorter FDB muscle fibers. We also show that the density of skeletal muscle sodium (Na^{+}) channels is also comparably greater in EDL muscle fibers than in FDB fibers. We hypothesize that the lower conduction velocity in the shorter FDB fibers provides comparable contractile synchrony in FDB fibers as is produced by higher conduction velocities in the longer EDL fibers. Part of this work was presented at the Biophysical Society Meeting, 2018.

MATERIALS AND METHODS

Ethical approval

All animals were housed in a pathogen-free area at the University of Maryland, Baltimore. The animals were euthanized according to authorized procedures of the Institutional Animal Care and Use Committee, University of Maryland, Baltimore, by regulated delivery of compressed CO_2 overdose followed by cervical dislocation.

FDB fiber preparation

FDB muscles were isolated from the hindlimbs of female CD1 mice between 4 and 8 weeks old. A total of 24 mice were used. Fibers were placed in 2 mg/mL type I collagenase/minimum essential medium (MEM) (Cat. No. 11095098; Gibco, Carlsbad, CA) to enzymatically dissociate single fibers for 4 h. Afterward, FDB fibers were also dissociated via mechanical means using a glass pipette in MEM with 0.1% gentamycin (Cat. No. G1397; Sigma, St. Louis, MO) and 10% fetal bovine serum (Cat. No. 100-106; Gemini Bio-Products, West Sacramento, CA). Multiple single fibers were plated on laminin-coated glass-bottomed dishes (Cat. No. P35G-1.0-14-C; Matek, Ashland, MA) in MEM with 0.1% gentamycin. Dishes were placed in a 37°C with 5% CO_2 incubator overnight. Cells were tested within 48 h of isolation.

Whole-muscle preparation for recordings

FDB and EDL muscles were isolated from the hindlimbs of female CD1 mice between 4 and 8 weeks old. A total of seven mice were used. Muscles were placed in a small petri dish containing warm L-15 media (Cat. No. 21083027; Life Technologies, Carlsbad, CA) supplemented with 0.1% gentamycin and 0.25% albumin. The ionic composition of L-15 is 137 mM NaCl, 5.7 mM KCl, 1.26 mM $CaCl_2$, and 1.8 mM $MgCl_2$ (pH 7.4). The muscles were loaded by adding 20 μM dihydrohod-2 (rhod-2) with 100 μM neostigmine, a cholinesterase inhibitor, to reduce the rate of cleaving of the dye by extracellular esterases (18). After 1 h of loading, the muscles were transferred to a glass-bottomed dish and held down using a plastic coverslip. The coverslip was secured using silicone grease (Chemplex 825; Fuchs Lubritech, Harvey, IL). Krebs' solution (112 mM NaCl, 25.7 mM $NaCO_2$, 4.9 mM KCl, 2.5 mM $CaCl_2$, 1.2 mM $MgSO_4$, 1.2 mM KH_2PO_4, 11.5 mM glucose, 10 mM HEPES) was then added to the glass-bottomed dish. Muscles were stimulated using 10 V/cm, 1 ms pulses while line scans were taken at a rate of 10,000 lines/s. Excitation for rhod-2 was provided by a 488 nm laser, and emitted light was collected at >505 nm. Muscles were imaged using either a 10× dry objective or a 60× water-immersion objective lens. Oxygenated (95% O_2, 5% CO_2) Krebs' solution was perfused across the dish throughout the recording session. Images were background corrected by subtracting an average value recorded outside the cell. The average fluorescence before stimulation was used to find F_0 (baseline before stimulation), which was used to scale the rhod-2 signal in the same region of interest (ROI) to obtain $\Delta F/F_0$ (change in fluorescence compared to baseline). Experiments were performed at room temperature, 21–23°C.

TT network imaging

Isolated cells were stained with 5 μM of di-8-ANEPPS in MEM for 2 h. Cells were kept in a 37°C incubator during this time. Excitation for di-8-ANEPPS was provided by a 543 nm laser, and emitted light was collected at >560 nm. The laser intensity was set to 20%. Cells were examined for structural integrity before being tested. Fibers were imaged using a 60× water-immersion objective lens with MEM as the recording solution. A set of four scans were taken at 3.5× zoom and averaged to produce each frame image. Images were background corrected to better display the TT network.

Whole mount muscle Na^{+} channel imaging

Extensor digitorum longus (EDL) and flexor digitorum brevis (FDB) muscles were dissected, stored in 4% paraformaldehyde, and labeled in parallel,

as previously described (19–22). Muscles were permeabilized using 0.5% Triton-X in phosphate-buffered saline (PBS) for 30 min at room temperature. After permeabilization, muscles were blocked with 8% goat serum in PBS for 1 h. Muscles were then incubated overnight with primary antibodies against Na_v 1.4 (rabbit anti-mouse at 1:250, SCN4A; Alomone Labs, Jerusalem, Israel) in 2% goat serum in PBS. Samples were washed with PBS three times for 10 min each. They were then incubated for 1 h at room temperature with α-bungarotoxin conjugated to Alexa Fluor 488 (1:200, B13422; Thermo Fisher Scientific, Waltham, MA) and goat anti-rabbit Alexa Fluor 647 (1:100, A-21244; Thermo Fisher Scientific). Samples were washed with PBS three times for 10 min each. Digital images of whole mount muscles were obtained using a confocal laser-scanning microscope (LSM Duo, Zeiss, Jena, Germany; pinhole size ~100 μm, 7.17 pixels/μm, 63× magnification). All image acquisitions were performed in a blinded fashion. Laser power, pinhole diameter, brightness, and other confocal microscopy parameters were fixed and not altered between samples. Imaging was performed at the level closest to the surface for all samples and approximately midway between the neuromuscular junction (labeled by α-bungarotoxin) and the muscle fiber end. Excitation for Na_v 1.4 and 4′,6-diamidino-2-phenylindole were provided by 633 and 405 nm lasers, respectively, and the emitted light was collected at >650 nm and >420 nm, respectively. Specificity of the antibody to Na_v 1.4 was confirmed with muscles (both EDL and FDB) imaged (data not shown) with only secondary antibodies (no incubation with primary antibodies to Na_v 1.4) and with Na_v-1.4-neutralizing peptide (Cat. No.: ASC-020; Alomone Labs). ROIs were user drawn and kept consistent across fibers. A background image containing no fibers was taken to estimate background fluorescence.

Di-8-ANEPPS voltage signal recording

Isolated fibers were stained with 5 μM of di-8-ANEPPS (Cat No. D3167; Invitrogen, Carlsbad, CA) in MEM for 2 h. Fibers were kept in a 37°C incubator during this time. MEM was aspirated and replaced with L-15 directly before testing. Fibers were stimulated at 17 V/com for 0.5 ms while line scans were taken at rates of either 10,000 lines/s or 50,000 lines/s (512 × 10,000 or 50,000 pixels). Records are an average of six scans from the same fiber at a given location. Tetrodotoxin (TTX, Cat. No. 554412; Millipore, Darmstadt, Germany) was administered at a 1 μM concentration. TTX was allowed 10 min after application to block Na^+ channels and obtain passive responses to stimulation. Excitation for di-8-ANEPPS was provided by a 532 nm laser, and emitted light was collected at >550 nm. To improve the signal/noise ratio, excitation light intensity was set to 20% of the 532 nm laser in the confocal system. To minimize photo damage, excitation light exposure was limited to 30 ms, beginning 3 ms before the start of the field stimulus. Fibers were examined for structural integrity and twitch responses to field stimulation before being tested. Fibers were imaged using either a 10× or 60× water-immersion objective lens with L-15 as the recording solution. Images were background corrected by subtracting an average value recorded outside the fiber. The average fluorescence before stimulation was used to find F_0 (baseline before stimulation), which was used to scale the di-8-ANEPPS signal in the same ROI to obtain $\Delta F/F_0$ (change in fluorescence compared to baseline). Experiments were performed at room temperature, 21–23°C.

Mag-fluo-4 Ca^{2+} recordings

Isolated fibers were loaded with 1 μM of mag-fluo-4 (Cat. No. M14206; Life Technologies, Eugene, OR) in 37°C L-15 (Cat. No. 21083027; Gibco) with 0.1% gentamycin and 0.25% albumin (Cat No. A8806-5G; Sigma-Aldrich) for 30 min. Media was aspirated and replaced with standard room temperature L-15 for 30 min before testing. Fibers were stimulated at 20 V/cm for 0.5 while line-scans (*xt*) were taken at a rate of 10,000 lines/s (512 × 10,000 pixels). Excitation for mag-fluo-4 was provided by a 488 nm laser. The emitted light was collected at >505 nm. Fibers were examined for structural integrity and twitch response to field stimulation before being tested for conduction velocity. Fibers were imaged using either a 10× or 63× water-immersion objective lens with L-15 as the recording solution. Images were background corrected by subtracting an average value recorded outside the cell (Fig. 2 *a*). The average fluorescence before stimulation was used to find F_0, which was used to scale the mag-fluo-4 signal in the same ROI to obtain $\Delta F/F_0$. Experiments were performed at room temperature, 21–23°C.

Alternate-polarity electric field stimulation and determination of AP conduction velocity

We used the membrane-impermeable, potentiometric dye di-8-ANEPPS to monitor changes in membrane potential in response to alternate-polarity electric field stimulation. The rationale is as follows. If we optically measure the AP using high time resolution (i.e., high-speed line scans) at both ends of the muscle fiber (Fig. 1 *a*), we can record the AP where it is initiated (at the negative facing end of the fiber) and the AP after it has propagated along the muscle fiber (at the positive facing end of the fiber). But this requires that we move the site of recording between ends of the fiber. Alternatively, we can switch the polarity of the bipolar electrodes and record line scans from the same end of the fiber for both negative and positive stimuli (i.e., for both depolarizing and hyperpolarizing field stimuli; Fig. 1 *b*). We then calculate the muscle fiber conduction velocity as

$$\text{Conduction velocity} = (L - 2a)/\left(t_{1/2}(+) - t_{1/2}(-)\right),$$

where L is the fiber length, a is the distance of the recording site from the nearby end of the fiber, and $t_{1/2}(+)$ and $t_{1/2}(-)$ are the times from start of the stimulus to half peak of the AP for an AP triggered respectively with the recording site in the fiber facing either the positive (Fig. 1 *c*, *top*) or negative polarity field electrode (Fig. 1 *c*, *bottom*). This approach avoids the need to record at two different spatial locations along the fiber to determine the AP conduction velocity.

As an orthogonal approach, in some fibers, AP conduction velocity was determined by using a single-polarity field stimulation but now recording APs at three different locations along the length of the fiber: near the end of the fiber facing the negative bath electrode, in the center of the fiber, and at the end of the fiber facing away from the negative electrode. The reciprocal of the slope of the line fit to $t_{1/2}$ values versus distance along the fiber gives the conduction velocity for these measurements.

If a muscle fiber is not oriented parallel to the electric field, it will only experience a fraction of the full field along its length. Consider a muscle fiber of length X oriented parallel to an electric field E. According to Fig. 1 *d*, in which X is the radius of a circle, if the fiber is oriented at an angle θ to the applied field, the fiber would experience an effective fractional component of the field (y/x) equal to $\cos(\theta)$ along its length, which is the effective longitudinal field for the fiber at angle θ to the field. In our experiments, we only record from fibers with $\theta \leq 45°$, in which case the fibers experience at least $\cos(45) = 0.71$ of the applied field.

Data analysis

Fluorescence time course data were acquired in LSM 5 Live (Zeiss), processed in Excel (Microsoft, Redmond, WA), and analyzed and plotted using OriginPro 2016 (OriginLab, Northampton, MA). Data following a normal distribution are presented as box plots indicating the range, Q1, mean, Q3 (*solid lines*), and median (*smaller box*), or as a column graph with error bars noting the mean ± standard error (SE). Where noted, a two-sample *t*-test or paired-sample *t*-test was used to test for significance (set at $p < 0.05$). Normality was evaluated using the Shapiro-Wilk test ($p < 0.05$: reject normality). For samples that had normality rejected, a Mann-Whitney test was performed (set at $p < 0.05$). Nonparametric data are represented as

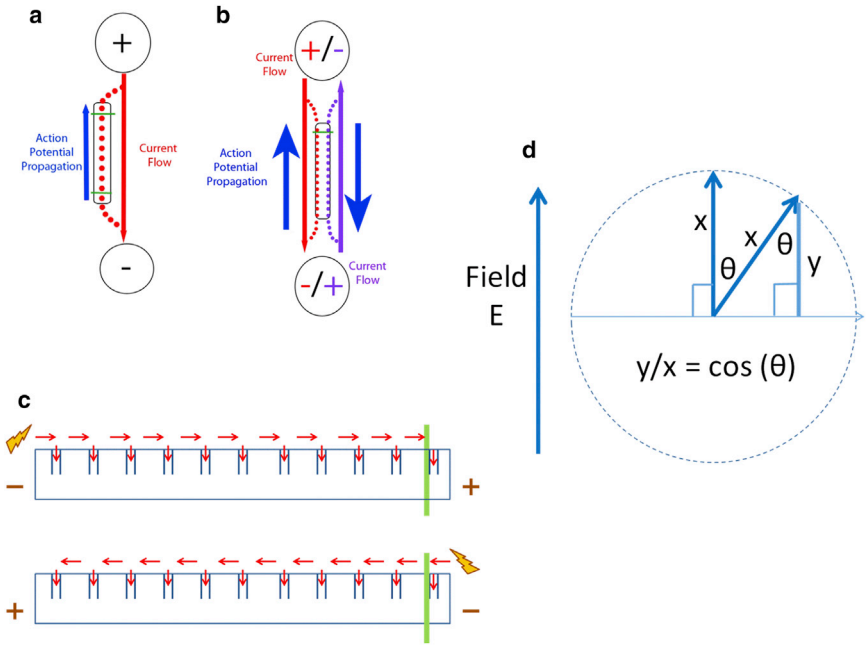

FIGURE 1 Effects of electric field generation on isolated muscle fibers. (*a*) Upon stimulation from a pair of external remote bipolar electrodes, the two ends of the muscle fiber will be affected in opposite ways. The end near the positive pole will be hyperpolarized (made more negative; V_m is measured by internal voltage relative to external voltage), whereas the end near the negative pole will be depolarized, and this is where the AP will be initiated. We can change our recording location from one end to the other end, thereby examining the initiation and propagation of the AP. (*b*) Alternatively, by changing the polarity of the electrodes, we can cause alternate depolarization of the fibers ends, thus alternating the location of the AP initiation while recording at the same fiber end, allowing for the measurement of propagation velocity of APs or AP-induced Ca^{2+} transients, providing that the fiber length is known. (*c*) A schematic showing direction of voltage propagation based on stimulation orientation. Stimulation (*lightning bolt*) will always begin at the side of the fiber near the negative electrode, propagating radially into the TTs as well as along the sarcolemma. We can record at one point along the fiber (*green line*), and switch the polarity of the electrodes, initiating an AP at either end of the fiber. (*d*) A vector diagram showing the effect of the electric field on muscle fibers when they are not parallel to each other. If within 45° of the field, fibers will experience at least cos(45) = 0.71 of the applied field. To see this figure in color, go online.

box plots indicating the range, Q1, Q3 (*solid lines*), and median (*smaller box*). TT network images were acquired using FluoView (Olympus, Center Valley, PA) and were processed using ImageJ (National Institutes of Health, Rockville, MD). Where mentioned, "m" represents the number of animals used in the experiment.

RESULTS

Two-dimensional visualization of TT network

Proper AP propagation requires a uniform, structurally intact TT network because the AP propagates longitudinally and radially through the TTs as well as along the sarcolemma. Di-8-ANEPPS binds to the cell membrane, diffuses into the t-system, and binds to the TT membrane. Thus, it can be used to measure the transmembrane potentials of both the surface membrane and TT network. Fig. 2 *a* shows an *xy* image of the TT network as shown via di-8-ANEPPS. At a 5 μM concentration of di-8-ANEPPS, the transverse tubules, as well as the longitudinal tubules, were well defined. Fig. 2 *b* shows a close up of a small section of the TT network and the normal "doublet" spacing between tubules. Fig. 2 *c* shows the fluorescence intensity profile of Fig. 2 *b*, which displays similar spacing.

Passive and active responses to 0.5 ms alternate-polarity field stimulation

Using field stimulation to elicit an AP will produce both passive and active electrical responses. The passive responses arise from electrotonic polarization of the membrane capacitance and resistance of the resting membrane, whereas the active responses encompass the AP triggered by the electrotonic depolarization. By applying di-8-ANEPPS (Fig. 3 *a*), we can optically record both types of membrane responses over time (Fig. 3, *b* and *c*). Because signals from di-8-ANEPPS are small, we averaged a total of six recordings of each polarity at each acquired location on the fiber to improve signal/noise ratios. A total of 30 fibers from 13 mice were included in this section of the study. As mentioned earlier, when recording from the ends of a fiber, stimulation will cause AP (4) initiation at the end of the fiber facing the negative field electrode, and the AP will conduct to the opposite end. When recording from the middle, however, the conduction delay is the same from both ends of the fiber, and there is no electrotonic polarization before the AP. Fig. 3 *b* displays example averaged recordings from both ends and the middle of the fiber for each polarity of field stimulation. TTX was applied after active responses were acquired to block AP initiation or propagation and isolate passive hyperpolarizations and depolarizations. Example recordings are displayed in Fig. 3 *c*. Previous studies have performed di-8-ANEPPS calibration tests using applied voltage steps (16,17). Both studies used a holding potential of −90 mV. Based on their studies, they estimated that the amplitude of APs observed through di-8-ANEPPS is approximately between 112 and 123 mV. This set of experiments shows that we can reliably examine changes in membrane voltage with di-8-ANEPPS.

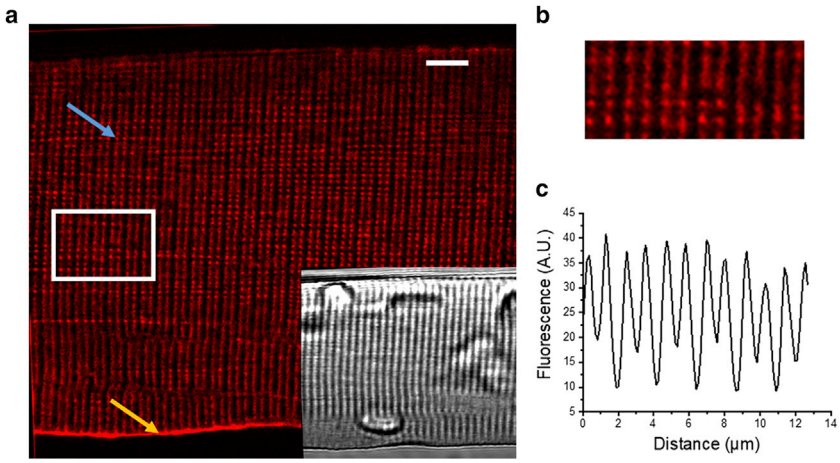

FIGURE 2 TT staining with di-8-ANEPPS. (*a*) A representative confocal image of a segment of an FDB fiber stained with di-8-ANEPPS to visualize the TT system. The calibration bar represents 5 μm. Transmitted light is shown in the inset. (*b*) A zoomed-in segment of the image in (*a*) indicated by the white box. (*c*) The graph indicates the average fluorescence intensity of thw boxed region shown in (*b*). The space between TTs is ~2 μm. The distance between the troughs represents the distance from Z line to Z line. Arrows indicate the location of regions of interest that could potentially be used to measure the time course of surface APs (*orange arrow*) or core APs (*blue arrow*) used in Fig. 3. To see this figure in color, go online.

AP longitudinal propagation velocity calculated from the difference in AP time courses recorded at the same end of a skeletal muscle fiber for opposite-polarity field stimulation

We have shown that we can optically obtain active responses from muscle fibers using field stimulation. With remote bipolar electrodes, we stimulated di-8-ANEPPS-stained muscle fibers with alternating polarity. As noted earlier, this allowed us to initiate an AP from either end of the muscle fiber. Utilizing this, we set out to estimate the AP conduction velocity by recording from one end and switching the stimulation polarity.

We calculated the conduction velocity using the difference in $t_{1/2}$ of the rising phases of the AP waveforms recorded at one end of the fiber during alternating-polarity stimulation and the muscle fiber length. By this method, we calculated the conduction velocity to be 0.39 $\pm$ 0.02 m/s. The average length of fibers was 446.2 μm (Table S1).

To check for run down (decay of signal throughout the experiment) and reproducibility during signal averaging,

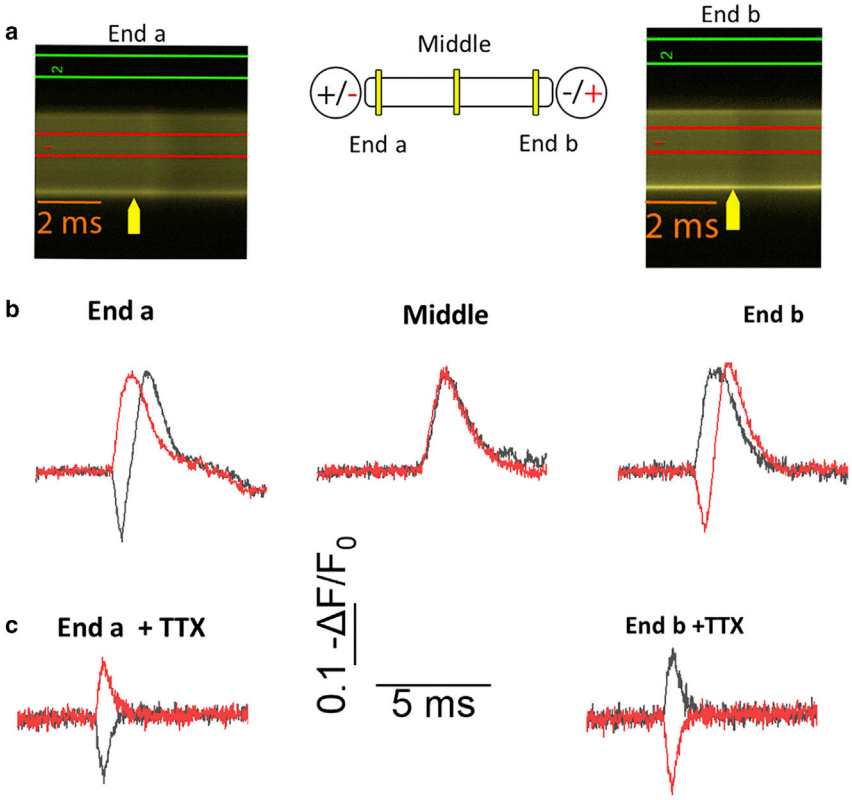

FIGURE 3 Potentiometric recordings at three locations using di-8-ANEPPS and alternating-polarity field stimulation. Averaged (n = 4) di-8-ANEPPS recordings from opposing ends of FDB fibers and the middle of the fiber are shown. (*a*) Example line scans from the same fiber on opposing ends. Red and green boxes show ROIs for the fiber and the background, respectively. Yellow arrows show the timing of stimulation. Even though the fiber exhibits an appreciable movement shortly after the stimulus, the sampled region of the line scan (within the *red lines*) remains within the fiber. (*b*) Averaged recordings from both ends and the middle of the same individual fibers. See text for fluorescence/voltage estimation. Yellow lines in the fiber cartoon show locations of line scan acquisition, ~50 μm from the ends of the fiber and the middle of the fiber. Note the lack of electrotonic potential in the middle recordings. Small movement artifacts can be seen after the end of the APs in these recordings. (*c*) Averaged (n = 2) di-8-ANEPPS recordings from the ends of the fibers in the presence of TTX. By blocking Na^+ channels, we can measure the passive properties of the muscle cells. To see this figure in color, go online.

F_0 during the first recording was compared to that of the final recording to determine the amount of bleaching (Fig. S1). This difference in F_0 was not found to be significant (Mann-Whitney, $p = 0.94$). Likewise, the peak $\Delta F/F_0$ of the first and last recordings on each polarity were compared to examine the signal rundown (Fig. S2). Again, these differences were found to be not significant (Mann-Whitney, positive polarity: $p = 0.56$; negative polarity: $p = 0.84$). These and the above results help show that the AP conduction velocity can be measured optically using di-8-ANEPPS to record APs at a single end of a muscle fiber together with alternating-polarity electrical field stimulation with bipolar electrodes.

Calculating AP propagation velocity from APs recorded at different locations with constant-polarity field stimulation

In addition to measuring conduction velocity by recording at a single location and switching the stimulating polarity, we can also move the recording site along the fiber, measure $t_{1/2}$ at different locations, and use the temporal differences with distance to calculate conduction velocity. We can plot $t_{1/2}$ against the length of the fiber and fit a line between those points. The slope of that line allows us to calculate conduction velocity using multiple points along the muscle fiber. Using this multipoint method, we calculated conduction velocity to be 0.45 ± 0.04 m/s, which is not significantly different from the velocity we calculated using the one-point method reported above using alternating-polarity stimulation (two-sample *t*-test, $p = 0.838$; Table S1). An example is shown in Fig. 4. We assumed that the latency between the pulse and $t_{1/2}$ is similar at each end of the fiber. When comparing these latencies, we did not find that difference to be statistically significant ($p = 0.47$).

Location of AP initiation

For our measurements to be valid, we must ensure that APs are starting at the end of the muscle fiber under our conditions and not some distance away from the end. We took high-speed frame scans of the ends of fibers loaded with mag-fluo-4 while being stimulated with either polarity nearby. We observe a clear initiation of the Ca^{2+} transient followed by the movement of the fluorescence out of the end of the fiber near the negative electrode at ~6.5 ms. In contrast, we see the Ca^{2+} transient flow into the end of the fiber when the fiber is stimulated on the opposite end near the negative electrode (Videos S1 and S2). We also took di-8-ANEPPS recordings from 50 to 100 μm away from the end of the fiber. The recordings look similar, but the 100 μm recording has a slightly delayed $t_{1/2}$ compared to the 50 μm recording, suggesting that the AP initiates at the end or at least within 50 μm from the end (Fig. 5).

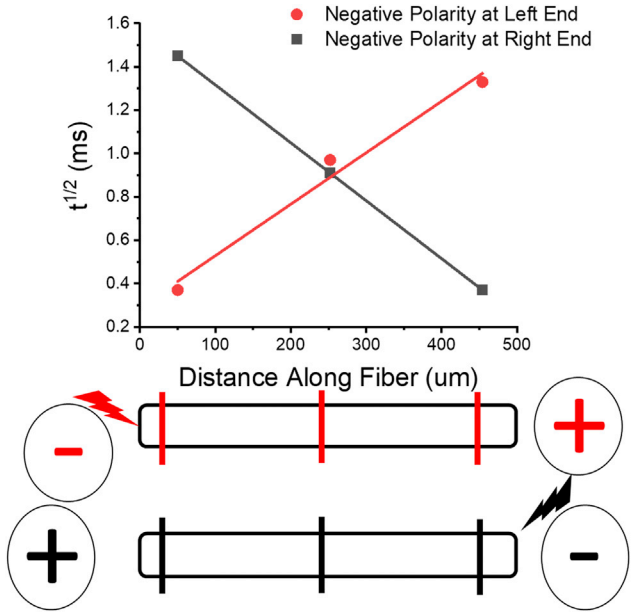

FIGURE 4 Recording conduction velocity using multiple points. For each polarity orientation (denoted by *red* or *black*), $t_{1/2}$ was recorded and plotted against the distance along the fiber. We fitted lines to those points and used the slopes to calculate conduction velocity. The muscle cartoon with red lines represents initiation from the "left" end of the fiber, and black lines from the "right" end of the fiber. To see this figure in color, go online.

Calculating AP longitudinal propagation velocity using Ca^{2+} signals for alternating polarity field stimuli

Voltage recordings with di-8-ANEPPS produce an observable electrotonic potential that will blend into the rising phase of the AP (Fig. 3). Furthermore, the signals are relatively small, so signal averaging is needed to increase the signal/noise ratio. In contrast, using the low-affinity Ca^{2+} indicator mag-fluo-4 produces a clear, easily observable record of the Ca^{2+} transient in a single (not averaged) record without any electrotonic potential from the field stimulus. As we have observed with the voltage signals, alternating-polarity stimulation produces a Ca^{2+} transient at the fiber end facing the negative electrode, which spreads to the opposing end because of the propagation of the AP depolarization (23). Because of this, we can also use AP-evoked Ca^{2+} transients to calculate the conduction velocity (Fig. 6). A total of 25 fibers from five mice were used in this portion of the study. We calculated the conduction velocity using the difference in $t_{1/2}$ of the rising phases of the AP-induced Ca^{2+} transients recorded at one end of the fiber during alternating-polarity stimulation. The conduction velocity, when measured via Ca^{2+} transients, is 0.37 ± 0.03 m/s. The average length of the fibers for these experiments was 436.6 μm. The difference in calculated conduction velocity between recordings performed using di-8-ANEPPS and mag-fluo-4 was not found

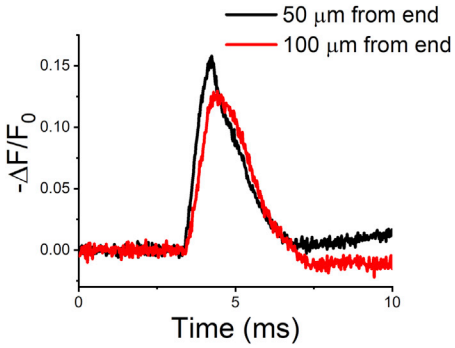

FIGURE 5 Di-8-ANEPPS recordings taken from 50 and 100 μm away from the end of the fiber initiating APs. By measuring rise time at two different locations, we can infer the location of initiation on the muscle fiber. The $t_{1/2}$ occurs later at 100 μm, suggesting that the AP initiates closer to the end of the fiber ($n = 5$). To see this figure in color, go online.

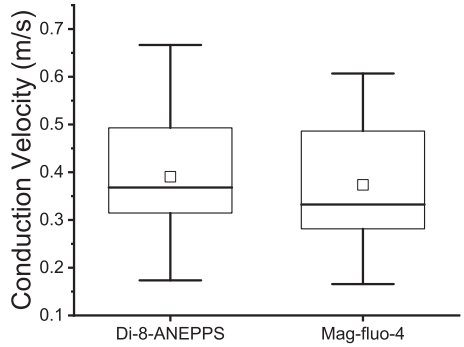

FIGURE 7 Conduction velocities measured by di-8-ANEPPS and mag-fluo-4. Box represents Q1, median, and Q3. Whiskers show the minimal and maximal values. Smaller box displays the mean. No significant difference was found between the two conditions (two-sample t-test, $p = 0.618$).

to be statistically significant (two-sample t-test, $p = 0.62$; Fig. 7). Thus, via remote bipolar electrodes, mag-fluo-4 can also be used to reliably measure the AP conduction velocity and provides a much clearer signal without any contribution from the electrotonic potential. In the presence of TTX, the AP is abolished, but the local electrotonic depolarization (at the end of the fiber facing the negative electrode) is sufficient to elicit a small Ca^{2+} transient (Fig. 6 *c*, TTX with initiation at near end).

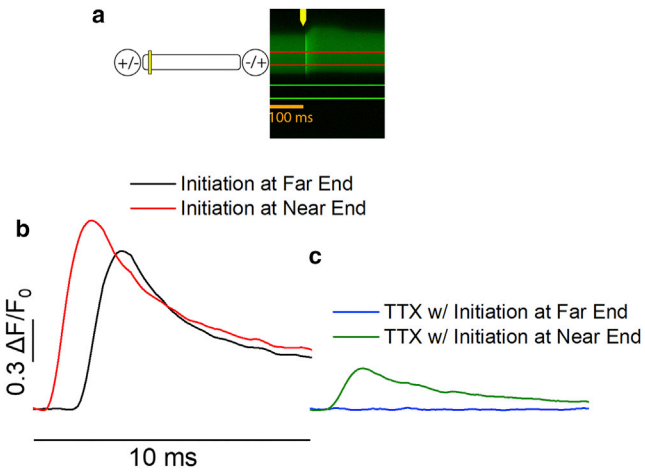

FIGURE 6 Example mag-fluo-4 recordings from one end of an FDB fiber. (*a*) The yellow line shows the relative location of line scan acquisition. An example line scan is shown with regions of interest for the fiber and the background (*red* and *green*, respectively). (*b*) The resulting time course plots from line scans of one fiber. The time difference between the $t_{1/2}$ of the transients allows us to calculate conduction velocity. Significant differences were found between the peak amplitudes of the transients elicited by the positive and negative polarities (paired-sample t-test, positive polarity: x = 1.15, negative polarity: 1.26, $n = 25$, $p = 0.03 \times 10^{-7}$). (*c*) Ca^{2+} recordings in the presence of TTX. If there is depolarization at the near end, there will be local release of Ca^{2+} because of the passive depolarization, but local release is not observed when the opposite end is depolarized. To see this figure in color, go online.

Detection of conduction velocity changes: Challenge with elevated extracellular potassium

To test whether our method was able to track changes in AP conduction, we experimentally challenged the muscle fibers to elevated extracellular potassium, a condition that is seen during muscle fatigue (24) and one that alters membrane potential (25,26), sodium channel gating, and Na^+-K^+ pump activity (24,27) and slows down AP conduction velocity (28). We hypothesized that a slight increase of the extracellular potassium concentration could decrease the conduction velocity in skeletal muscle. Using mag-fluo-4, we tested the conduction velocity of each selected fiber first in our standard recording solution (L-15), which has a 5.7 mM concentration of KCl, then switched the media to a modified L-15 solution with 7.5 mM KCl and tested at 5, 10, and 20 min after altering the KCl content (Fig. 8 *a*). At 5 min, we measured a significant decrease in conduction velocity in the elevated KCl group ($n = 11$) compared to control (Mann-Whitney, $n = 15$, $p = 0.00309$). This change persisted at 10 (Mann-Whitney, $p = 0.0002$) and 20 min (Mann-Whitney, $p = 0.0001$, Fig. 8 *b*; Table S2). Some of the cells became too depolarized to initiate Ca^{2+} transients at later time points and were removed from the analysis. Fibers exposed to a mock solution change (replacing the original 5.7 mM K solution) showed no significant change in conduction velocity at 5, 10, or 20 min (representative traces shown in Fig. 8 *a*, full data not shown). These findings show that we can reliably track changes in conduction velocity using our methods.

Conduction velocity in longer skeletal muscle fibers

Although we can reliably track changes in conduction velocity in FDB muscle fibers using our novel, to our knowledge, methods, we noticed that the speed of propagation is considerably slower than what has been previously reported

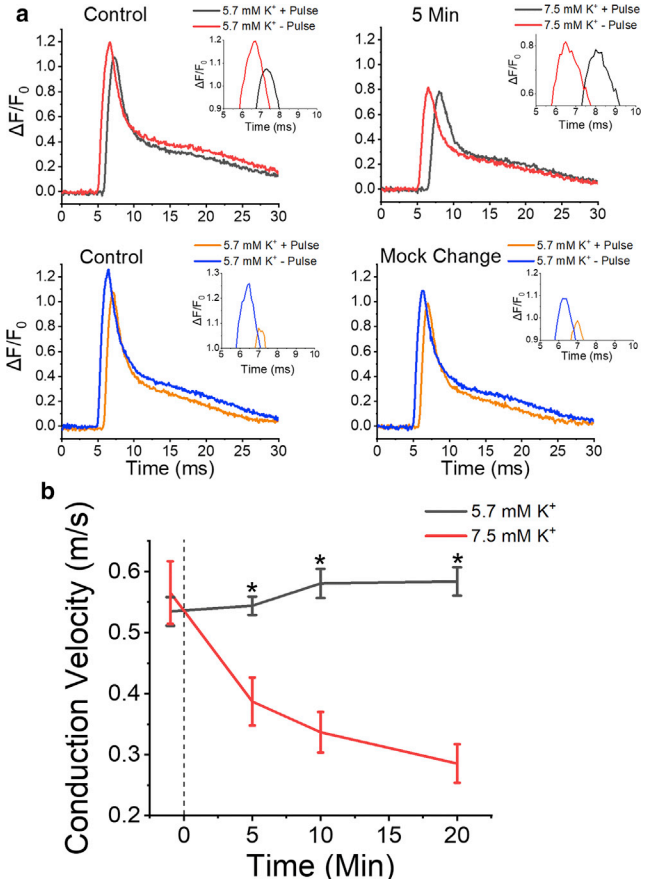

FIGURE 8 Conduction velocity measurements from wild-type fibers in 5.7 and 7.5 mM KCl using mag-fluo-4. (*a*) Example Ca^{2+} transients from fibers in 5.7 and 7.5 mM KCl fibers. The inset shows a zoom-in the timing of the full peak between transients recorded at the end of initiation versus the end of propagation. Fibers are shown before the solution switch and 5 min afterwards. (*b*) Line and symbol plots show average changes in conduction velocity over time. Fibers that did not respond after an increase in KCl were removed. The dotted line indicates when solution was changed. Asterisk indicates significance established using a one-way analysis of variance, 5.7 mM ($n = 15$) vs. 7.5 mK KCl ($n = 11$). Pre-switch, $p = 0.553$; 5 min, $p = 0.0003$; 10 min, $p = 0.000002$; 20 min, $p = 0.00000004$). To see this figure in color, go online.

for other muscle groups (29). We thus wanted to also measure conduction velocity in longer muscle fibers. We hypothesize that to maintain contractile synchrony, longer muscle fibers require a faster conduction velocity. Unlike our other recordings using single muscle fibers, we made these recordings using the whole excised FDB or EDL muscles, visualizing individual fibers within the bundles. This not only allows us to rule out potential deleterious effects of the enzymatic fiber isolation but is also more physiologically representative. The EDL fibers examined were 1.28 ± 0.0018 mm long. Using rhod-2, we visualized Ca^{2+} transients for APs starting at either end of the muscle fibers in the whole muscle using alternating-polarity electric field stimulation. Our results revealed a significantly greater conduction velocity in EDL fibers than in FDB fibers (one-way analysis of variance, $p = 0.0001$, Fig. 9). Importantly, when comparing our whole-muscle FDB fiber results to our single-fiber results, we saw no significant difference between the average conduction velocities (two-sample *t*-test, $p = 0.240$, Fig. 11).

Na^+ channel expression levels in fibers of different lengths

Voltage-gated Na^+ sodium channels (Na_v 1.4) play an essential role in skeletal muscle and are responsible for the longitudinal and radial propagation of the AP (30,31). One conceivable explanation for a difference in conduction velocity between shorter and longer muscle fibers could be a difference in Na_v 1.4 expression. Fig. 10 shows representative confocal images of regions of whole FDB or EDL stained for Na_v 1.4 expression. A negative control is shown in Fig. S3. After examining at the TT and sarcolemmal levels, we observed a significantly higher level of channels on the EDL fibers than the FDB fibers (two-sample *t*-tests, $p = 0.024$, $p = 0.005$, $n = 3$, m = 2, Fig. 10 *b*). A previous study has also shown this difference using Western blots (32). These findings suggest that a higher concentration of Na^+ channels could be at least partially responsible for the observed differences we see in conduction velocity between the muscle groups.

Modeling passive response of fiber to electric field stimulation by remote bipolar electrodes

Our novel, to our knowledge, method of calculating AP conduction velocity assumes that APs are initiated at the end of the muscle fiber facing the negative electrode. We created a model circuit diagram for the passive electrical properties of the muscle fiber to predict the pattern of depolarization during field stimulation from remote bipolar electrodes.

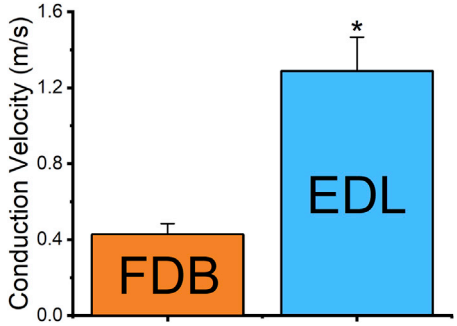

FIGURE 9 Conduction velocity in FDB fibers and EDL fibers. Column graphs showing mean velocities in whole FDB and EDL. Recordings were made using rhod-2 in the whole muscle. Muscles were dissected out, loaded, and kept in place using a coverslip and silicone grease. Bars represent the mean ± SE. EDL fiber conduction velocity was found to be significantly greater than that of FDB fibers ($p = 0.0001$). To see this figure in color, go online.

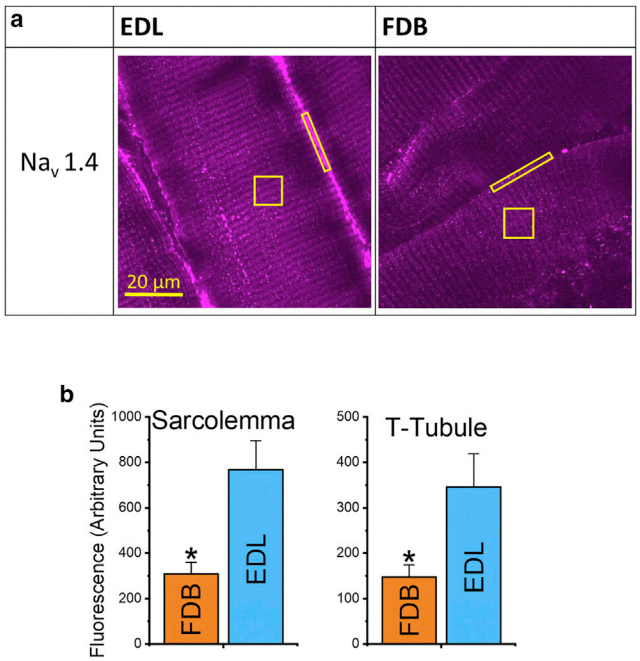

FIGURE 10 Na^+-channel-derived fluorescence from whole mounts of EDL and FDB. (*a*) Example images of FDB and EDL whole mount with Na^+ channels labeled. Yellow boxes indicate example regions of interest on the sarcolemma (*rectangular*) and in the TT (*square*). (*b*) A column graph showing the mean fluorescence intensities due to Na^+ labeling at the sarcomere (*left*) and TT (*right*). Bars represent the mean ± SE. EDL fiber fluorescence was significantly higher than that of FDB fibers at both the sarcolemma ($p = 0.005$) and the TT ($p = 0.024$). To see this figure in color, go online.

We assume that in the immediate vicinity of a muscle fiber plated in the culture dish, the following apply:

1) The electric field generated in the bath by the remote bipolar stimulating electrodes is constant (i.e., the voltage changes linearly with distance along the direction of the field),
2) The local electric field generated by the stimulating electrodes is locally spatially uniform in the vicinity of the fiber, and
3) The presence of the fiber causes negligible change in the voltage generated in the bath by the stimulating electrodes.

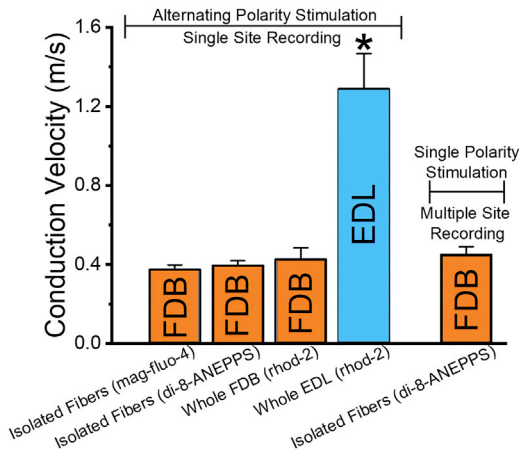

FIGURE 11 Conduction velocities from FDB fibers and EDL fibers under various conditions. The measurements on the right were taken using single-polarity stimulation and multiple site recording, whereas the four other conditions were made using alternating-polarity stimulation and single-site recording. Error bars represent the SEM. To see this figure in color, go online.

Under these assumptions, the voltage outside the fiber will change linearly with distance along the fiber. If the fiber is exactly parallel to the field, the voltage gradient along the fiber will be the full voltage gradient parallel to the field. If the fiber is at an angle to the applied field, the voltage along the fiber will still change linearly with distance along the fiber, but voltage change per unit fiber length will be less than the full field by a geometric factor that depends on the fiber angle. In the fibers studied here, the fiber is within 45° of the field direction, so the field component along the fiber is greater than 70% of the total field (see Materials and Methods). In all cases, we use the corresponding voltage applied to the low bath resistance to generate a linear voltage change along the outside of the fiber. We apply the extracellular voltage profile to a linear cable model of the fiber (Fig. 12 *a*) to calculate the fiber membrane potential as a function of time and location within the fiber.

Our analysis considers only fiber polarization due to the component of the applied electric field that is parallel to the long axis of the fiber. Fiber polarization due to the transverse component of the electric field is smaller because it only corresponds to a shorter distance (the fiber diameter) along the transverse field, in contrast to the fiber length, which is subjected to the longitudinal component of the electric field. Transverse polarization is likely to be seen only in fibers oriented close to perpendicular to the applied field (23) or in fibers intentionally stimulated transversely using long electrodes parallel to the fiber (15).

Passive cable model of an isolated skeletal muscle fiber in a large bathing solution

We developed a lumped circuit model to simulate the passive electrotonic polarization of a muscle fiber due to electric field stimulation. For our simulation, we divided the fiber into seven lumped membrane elements, each of which consists of a membrane resistance component (R_{memb}) in parallel with a membrane capacitance component (C_{memb}). Each membrane element represents a length l, which is 0.143 of the total fiber length L. Each membrane element connects the bathing solution, where the bath electric field is generated by the applied field stimulus, to the fiber interior. Neighboring membrane elements are separated from each other inside the fiber by an internal longitudinal resistance element (R_{int}) and are separated from each other outside the fiber by an external longitudinal resistance

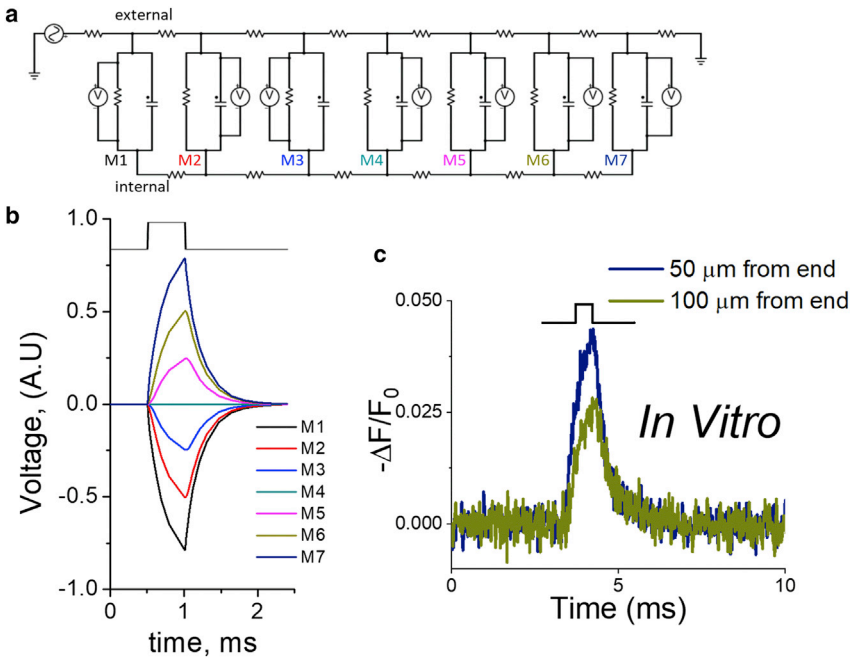

FIGURE 12 Circuit diagram for modeling the passive properties of FDB muscle fibers. (*a*) A diagram was made via PartSim. The diagram was made to contain seven identical elements. We have also constructed a model of a fiber 10 times longer. In the 10× model, the passive depolarization and hyperpolarizations have a larger amplitude closer to the ends, similar to this model, but there is a long segment in the middle in which no changes in voltage are observed (data not shown). The measuring points are color coded with the line graph in (*b*), M1–M7; M4 is the element in the middle of the fiber. The values used for r_m and c_m, the membrane resistance times unit fiber length and capacitance per unit fiber length, and r_i, the fiber internal resistance per unit length, are $r_m = 0.25$ MΩ mm, $c_m = 8.8 \times 10^{-6}$ μF/um, and $ri = 1.2$ MΩ/mm, similar to those reported in (28,29). (*b*) Example passive responses from the seven element diagram. A 20 V pulse lasting 0.5 ms was applied to the circuit. The end of the circuit closer to the battery experiences depolarization, which degrades as the recording points move away from the battery. At the halfway point (M4-c), no voltage is recorded, but beyond that point a passive hyperpolarization is seen and increases until the end of the circuit. (*c*) Recordings of passive properties at 50 and 100 μm from the end of FDB fibers. Passive depolarization, similarly to our model recordings, is lower as we examine closer to the middle of the fiber. To see this figure in color, go online.

element (R_{ext}). Note that there are no internal resistance units at the two internal ends of the fiber and that the external resistance at the ends of the fiber are connected, via appropriate bath resistances, to the field-stimulation electrodes (above). The external longitudinal resistance is set very low to maintain the constant field in the bath despite the presence of the fiber (condition 3, above).

For this simulation, L was assumed to be 490 μm in length, close to the average length of fibers in these experiments. Each of the seven membrane components, and each of the internal resistance elements then represents a 70 μm length of fiber, and each of the external resistances represents the electrical properties of the bath corresponding to 70 μm of the fiber. The circuit element values are $R_{int} = r_i l$, $R_{memb} = r_m/l$, and $C_{memb} = c_m l$, where r_m and c_m are the membrane resistance times unit length and capacitance per unit fiber length and r_i is the fiber internal resistance per unit length. The values of the circuit elements were calculated from values of fiber internal resistance per unit length, membrane resistance times the unit length, and membrane capacitance per unit length determined from studies describing electrical cable properties of mouse EDL skeletal muscle fibers (33,34). See Fig. 12 legend for the values of r_m, c_m, and r_i used in our simulations. Note that the membrane elements in our cable model of the fiber ignore the effects of resistance in series with the TTs' membrane capacitance, which we have not considered in our simulations.

Simulations were done by applying a voltage step across the two end terminals of the extracellular series of resistances (Fig. 12 *a*) and calculating the resulting voltage time course across each transmembrane element using the circuit solving software PartSim (AspenCore, Garden City, NY). For a 0.5 ms pulse applied to the bath via the field-stimulating electrodes (Fig. 11 *b*, *top*), the model exhibits a brief (0.5 ms) electrotonic depolarization at the fiber end nearest the negative electrode (Fig. 12 *b*, largest positive response) and an equal but opposite polarity hyperpolarization at the end closest to the positive electrode (Fig. 12 *b*, largest negative response), as is observed when an actual muscle fiber with Na^+ conductance blocked or eliminated is subjected to alternate-polarity 0.5 ms field stimuli (Figs. 3 and 12). There is no electrotonic potential across the membrane elements at the fiber center, and successively decreasing polarization (depolarizing or hyperpolarizing) moving from the ends to the central elements, respectively. Thus, the field stimulus produces graded depolarization over the half fiber facing the negative electrode and graded hyperpolarization over the half facing the positive electrode, with maximal polarization at the fiber ends and none at the center. We observe similar depolarization and hyperpolarization at opposite ends of the muscle fibers in vitro using our experimental system, indicating that our cable model is appropriate (Fig. 12 *c*). At present, we have restricted the model to demonstrate the cable properties at seven 70-μm-length fiber segments (Fig. 12), but we are able to increase the length to test how these properties change with an increase in length. This model will help us quickly and reliably test the passive properties of different lengths and diameters of

skeletal muscle fibers, allowing us to estimate what will happen to skeletal muscle fibers in vitro in the absence of fiber excitability.

DISCUSSION

Our optical noninvasive studies using the potentiometric dye di-8-ANEPPS combined with high temporal resolution allow us to directly examine the passive and active voltage changes in response to field stimulation. Bipolar stimulation enables us to initiate APs at either end of the muscle fiber, which allows us to optically record the AP conduction velocity while recording only at a single end of the fiber. In addition, we are also able to examine conduction velocity with Ca^{2+} indicators. Previous research in our lab suggests that in the absence of AP initiation, the passive depolarization caused by bipolar field stimulation results in localized Ca^{2+} release at the end of the fiber facing the cathode (23). This is dependent on the stimulation polarity and results from a direct activation of the Ca_v 1.1 channels, the voltage sensors of the excitation-contraction coupling, at the depolarized end of the fiber and the subsequent nonpropagated Ca^{2+} release (23). Our current results support this finding. In our mag-fluo-4 recordings in the presence of TTX, a small amount of Ca^{2+} release can be seen at the fiber end facing the cathode (Fig. 4), showing that passive depolarization indeed causes local Ca^{2+} release. In agreement with this observation, our model confirms some features of the electrotonic responses seen in the single muscle fibers. External field stimulation causes depolarization in the half fiber facing the negative electrode and hyperpolarization over the half facing the positive electrode.

Because conduction velocity of skeletal muscle is affected by different pathological conditions (5–9), developing a method that allows for this quantification represent an important addition to the battery of tools used to investigate muscle function. This approach can be used to quickly and noninvasively obtain details about the muscle fiber excitability and AP properties. The advantage of the utilizing bipolar electrodes with the field roughly parallel to the fiber is that it elicits AP longitudinal propagation that resembles the natural spread of the AP along the fiber in situ, in contrast to the quasi-instantaneous longitudinal activation obtained with electrodes running 45° off the longitudinal axis of the fiber (15). Manno et al. used FDB fibers and high-speed imaging of di-ANEPPS signals to evaluate AP trajectories simultaneously at multiple locations along the TT system and to estimate AP radial propagation using shifted excitation and emission ratioing, which relies on a more elaborate setup (14). Our system allows for the screening of individual muscle fibers' AP properties occurring at both the surface and TT system. The AP can be monitored simultaneously at multiple locations while allowing for high time and spatial resolution using a nonratiometric approach with similar sensitivity to that offered by ratiometric approaches.

Optical recordings have their pitfalls as well. Estimating waveforms and conduction velocity from *xt* line scan images means that our temporal resolution is only as high as our line acquisition rate. In some microelectrode amplifiers, the sampling rate can be similar or higher than in optical recordings. Additionally, the di-8-ANEPPS signal itself is weaker than that of Ca^{2+} indicators, and although di-8-ANEPPS is a potentiometric dye, it is not very voltage sensitive. A previous report showed that di-8-ANEPPS only has a fluorescence change of 2.5% per 100 mV change (35). Using shifted excitation and emission ratioing, Manno et al. were able to attain di-8-ANEPPS sensitivities between 27 and 35% per 100 mV (14). To improve the signal/noise ratio, we took multiple recordings and averaged them (synchronized with the field stimulus pulse).

Mag-fluo-4 is much more sensitive to changes in Ca^{2+} than di-8-ANEPPS is to changes in voltage. Mag-fluo-4 provides a much clearer signal, without requiring averaging of multiple recordings. However, the propagation speed of Ca^{2+} transient is a derivate estimate of AP conduction. It is possible that as voltage travels along the membranes, the delay between the AP and Ca^{2+} transient could change. Therefore, for these measurements to maintain strict validity, we must assume that the delay between APs and Ca^{2+} transients is the same at both ends of the fiber. However, the close agreement of the conduction velocities measured with di-8-ANEPPS and mag-fluo-4 indicates that requirement is fulfilled.

Previous studies that have examined sarcolemmal conduction velocity (i.e., the longitudinal conduction velocity along the muscle fibers) in humans found much higher values, up to 6.4 m/s (28,36). The radial and longitudinal conduction velocity in the TT is much slower (14,15,37). Our values for the AP propagation velocity along the sarcolemma are over an order of magnitude larger than the speed of longitudinal propagation along the longitudinal TT system (as reported for "skinned" muscle fibers). Because propagation of the AP along the sarcolemma is so much faster than propagation along the longitudinal TT system, we hypothesize that the determining factor for longitudinal AP conduction velocity in intact muscle fibers is the velocity of the sarcolemma AP.

Conduction velocity analyses in frog muscle have shown much higher speeds than what we observed in our studies. A classic study using winter and spring frogs found average conduction velocities of 2.44 and 2.05 m/s, respectively (38). Conduction velocity is known to increase with fiber diameter and length, and the average frog muscle is much larger than the mouse muscles we observed in our studies. Studies in rat have also shown higher values than what we recorded. A study from Kupa and colleagues calculated the conduction velocity in rat EDL fibers to be 3.02 m/s on average and 1.70 m/s on average in the soleus (10).

The AP conduction velocity of 0.39 m/s obtained here in mouse FDB muscle fibers is about an order of magnitude

lower than the values 3.5 and 3.8 m/s previously reported for mouse sartorius (39) and EDL (28) muscle fibers. A key difference between the fibers studied here and those described in earlier reports is that FDB fibers are much shorter than the previously studied fibers. In a much shorter fiber, a proportionally slower AP can produce a similarly synchronized depolarization at the fiber ends as produced by a proportionally faster AP in a much longer fiber. Thus, slower conduction is sufficient for near-synchronous activation of the relatively short FDB fibers used here.

In our examination of EDL fibers, we observed a faster conduction velocity compared to that of FDB fibers as recorded under the same experimental conditions, which lends support to our hypothesis of the necessity of contractile synchrony. We also found a greater expression of Na_v 1.4 channels on the sarcolemma and in the TT network of EDL fibers, providing one possible explanation for the discrepancy in conduction velocity. A slower conduction velocity due to a lower level of membrane Na^+ channels would decrease Na^+ influx, and lower concentrations of Na^+ channels have been associated with less fatigability (40). We thus hypothesize that short muscle fibers may be specialized to use more slowly propagating APs for energy conservation.

A lower Na^+ channel density in FDB fibers could also explain their relatively high sensitivity to K^+ depolarization. We have observed a decreased conduction velocity to ~49% of control and some failure of excitation for the modest increase of extracellular [K^+] from 5.7 to 7.5 mM in FDB fibers (Fig. 6). Furthermore, we found that 10 mM extracellular [K^+] completely eliminated excitability of FDB fibers (data not shown), which was not observed in reports on longer muscle fibers from mice (28). The increased susceptibility of FDB fibers to suppression of excitability by elevated extracellular K^+ would be consistent with a lower level of Na^+ channel membrane expression in FDB fibers compared to longer muscle fibers. Our recording temperature also could have had a significant effect on our obtained values. A previous report showed that when rat EDL fibers are kept at 35°C, conduction velocity is slightly under 3.0 m/s. However, if the temperature is reduced to 22°C, the conduction velocity goes down to a little over 1.0 m/s (29).

Our recordings with both di-8-ANEPPS and mag-fluo-4 provided similar values for the longitudinal conduction velocity. The membranes of the TT and the sarcoplasmic reticulum (SR) are molecularly coupled (41), and TT membrane depolarization leads to activation of the SR Ca^{2+} release channels (42). SR Ca^{2+} release cannot occur without TT voltage propagation. Because of the small time window between depolarization, Ca^{2+} release, and the mag-fluo-4 signal, and by extension Ca^{2+}, we can also use the mag-fluo-4 signal to estimate the AP conduction velocity. In our testing conditions, we observed that both mag-fluo-4 and di-8-ANEPPS are useful tools to measure AP conduction velocity. Although we did not observe any significant differences between Ca^{2+} and voltage propagation, we cannot guarantee this will be the case in every experimental condition.

When field-stimulating fibers using remote bipolar electrodes as under these conditions, we must take the angle of the fiber relative to the electric field into account. In our diagrams (Fig. 1), the fiber is oriented parallel to the line between the two electrodes. When in this orientation, the fiber experiences the largest electrotonic electrical polarization during field stimulation. As the fiber rotates away from parallel, the amplitude of the electrotonic potentials decreases until the fiber is perpendicular to the electric field, in which it is least responsive because of zero electrotonic potential at the fiber ends but with a small transverse polarization due to the field that is now across the fiber. Using different types of electrode geometry will generate different electric fields, eliciting different responses. If we use a focal electrode, we can elicit depolarization from any point along the fiber, from which an AP would propagate in both directions (23).

A previous study from our lab characterized the behavior of fibers that only contract and display Ca^{2+} transients at one end when stimulated with a given polarity (23). If a fiber only twitches at one end, it cannot be used for conduction velocity measurements using mag-fluo-4. There will only be local Ca^{2+} release at the twitch site and no local or propagated AP. However, alternating fibers can still be used to examine the passive electrical properties of the fiber using di-8-ANEPPS. The electrotonic potential will still be produced in alternating fibers. Whether using alternating fibers or uniformly contracting fibers, our approaches can show the passive and/or active properties of skeletal muscle fibers, using either mag-fluo-4 or di-8-ANEPPS.

In our experiments with fibers challenged with extracellular elevated K^+, we observed that conduction velocity slowed in a time-dependent manner. In fatigue states, in which extracellular K^+ is elevated, the cell membrane is partially depolarized, the sodium permeability is reduced, and the ability to generate APs is decreased. We suspect that something similar is happening in our conditions as well, despite the lack of K^+ efflux from the intracellular milieu. KCl is a known membrane depolarizer, and the depolarization effect should occur immediately. Furthermore, a notable percentage of the fibers became unable to generate APs, even at just 7.5 mM KCl. This percentage also increased with time. Regardless, these changes demonstrate that we can track alterations in conduction velocity using fluorescent dyes coupled with field stimulation.

Overall, this approach allows us to attain good signal/noise ratios using di-8-ANEPPS. This approach can also be applied to other cell types, such as cardiac fibers or axonal projections. There are some relatively new voltage or Ca^{2+}-sensitive sensors that could work very well in tandem with our method. Genetically engineered fluorescent probes have been shown to be useful and efficient in

measuring membrane potential and Ca^{2+} changes. ASAP1, a fast voltage sensor (43), and G-CaMP, a genetically encoded Ca^{2+} probe (44), have been shown to be effective in neurons (45); however, the time response of di-8-ANEPPS (<1 ms) is superior to that of genetically encoded voltage or Ca^{2+} probes. Yet, because of dye uptake and delocalization, di-8-ANEPPS is not suitable for long-term experiments (>4 h).

CONCLUSIONS

To summarize, we have determined the AP conduction velocity under control conditions from single-site optical recording with alternating-polarity electric field stimulation using several dyes. For FDB fibers, we found a value very close to 0.4 m/s with isolated FDB fibers and either the Ca^{2+}-sensitive dye mag-fluo-4 or the membrane-potential-sensitive dye di-8-ANEPPS, as well as when using fibers in whole FDB muscles loaded with the Ca^{2+} indicator rhod-2 (Fig. 11, *left* three bars). In contrast, alternating field stimulation with EDL fibers loaded with rhod-2 in whole EDL muscle gives a more than threefold larger conduction velocity for EDL fibers than for FDB fibers (Fig. 9). For reference, multiple location recording with single-polarity stimulation of isolated FDB fibers gives essentially the same conduction velocity as obtained from the single-site recording experiments with alternating-polarity stimulation on isolated FDB fibers or on FDB fibers in whole FDB muscle (Fig. 11, *right bar*). Taken together, these results validate the single-site recording approach and establish a more than threefold lower AP conduction velocity in FDB fibers than in EDL fibers.

We have demonstrated that di-8-ANEPPS or mag-fluo-4 can be used to measure the AP conduction velocity using high-speed optical recording at one end of the fiber together with alternating-polarity field stimulation from remote bipolar electrodes. We anticipate that this novel, to our knowledge, but simple method could be an important additional research tool to reexamine skeletal muscle components of neurological diseases such as amyotrophic lateral sclerosis, Alzheimer's, and Huntington's (46–48).

SUPPORTING MATERIAL

Three figures, two tables, and two videos are available at http://www.biophysj.org/biophysj/supplemental/S0006-3495(18)31215-3.

AUTHOR CONTRIBUTIONS

Q.B. performed majority of in vitro experiments and wrote majority of the paper. S.J.P.P. performed the initial experiments, testing experimental design. S.R.I performed the whole mount staining of muscles and edited drafts of the paper. R.M.L. edited drafts of the paper. E.O.H gave experimental advice throughout the experimental process, helped design the approaches for various experiments, designed the circuit model, and provided edits for the paper. M.F.S. conceptualized the project, designed the approach, designed the circuit model, wrote the section of the paper on the circuit model, provided edits for the paper, and gave experimental advice throughout the process.

ACKNOWLEDGMENTS

Research reported in this publication was supported by the National Institute of Arthritis and Musculoskeletal and Skin Diseases of the National Institutes of Health under Award Number R37AR055099 (to M.F.S.). Q.B. was supported by National Institute of Arthritis and Musculoskeletal and Skin Diseases-National Institutes of Health training grant T32 AR007592 to the Interdisciplinary Program in Muscle Biology, University of Maryland School of Medicine.

REFERENCES

1. Rosenfalck, P. 1969. Intra- and extracellular potential fields of active nerve and muscle fibres. A physico-mathematical analysis of different models. *Acta Physiol. Scand. Suppl.* 321:1–168.
2. Katz, B. 1966. *In* Nerve, Muscle, and Synapse, *Volume 1*, Fifth Edition. McGraw-Hill Higher Education, New York.
3. Sheikh, S. M., J. N. Skepper, …, C. L. Huang. 2001. Normal conduction of surface action potentials in detubulated amphibian skeletal muscle fibres. *J. Physiol.* 535:579–590.
4. Coronel, R., D. H. Lau, …, M. R. Rosen. 2010. Cardiac expression of skeletal muscle sodium channels increases longitudinal conduction velocity in the canine 1-week myocardial infarction. *Heart Rhythm.* 7:1104–1110.
5. Mense, S., and M. Stahnke. 1983. Responses in muscle afferent fibres of slow conduction velocity to contractions and ischaemia in the cat. *J. Physiol.* 342:383–397.
6. Van der Hoeven, J. H., M. J. Zwarts, and T. W. Van Weerden. 1993. Muscle fiber conduction velocity in amyotrophic lateral sclerosis and traumatic lesions of the plexus brachialis. *Electroencephalogr. Clin. Neurophysiol.* 89:304–310.
7. Almeida, S., M. C. Riddell, and E. Cafarelli. 2008. Slower conduction velocity and motor unit discharge frequency are associated with muscle fatigue during isometric exercise in type 1 diabetes mellitus. *Muscle Nerve.* 37:231–240.
8. Cadore, E. L., M. González-Izal, …, M. Izquierdo. 2014. Muscle conduction velocity, strength, neural activity, and morphological changes after eccentric and concentric training. *Scand. J. Med. Sci. Sports.* 24:e343–e352.
9. Suda, E. Y., A. A. Gomes, …, I. C. Sacco. 2016. Muscle fiber conduction velocity in different gait phases of early and late-stage diabetic neuropathy. *J. Electromyogr. Kinesiol.* 30:263–271.
10. Kupa, E. J., S. H. Roy, …, C. J. De Luca. 1995. Effects of muscle fiber type and size on EMG median frequency and conduction velocity. *J. Appl. Physiol. (1985).* 79:23–32.
11. Broman, H., G. Bilotto, and C. J. De Luca. 1985. Myoelectric signal conduction velocity and spectral parameters: influence of force and time. *J. Appl. Physiol.* 58:1428–1437.
12. Pratt, F. H. 1917. The all-or-none principle in graded response of skeletal muscle. *Am. J. Physiol.* 44:517–542.
13. Vergara, J., and F. Bezanilla. 1976. Fluorescence changes during electrical activity in frog muscle stained with merocyanine. *Nature.* 259:684–686.
14. Manno, C., L. Figueroa, …, E. Ríos. 2013. Confocal imaging of transmembrane voltage by SEER of di-8-ANEPPS. *J. Gen. Physiol.* 141:371–387.
15. Edwards, J. N., T. R. Cully, …, B. S. Launikonis. 2012. Longitudinal and transversal propagation of excitation along the tubular system of rat fast-twitch muscle fibres studied by high speed confocal microscopy. *J. Physiol.* 590:475–492.

16. DiFranco, M., J. Capote, and J. L. Vergara. 2005. Optical imaging and functional characterization of the transverse tubular system of mammalian muscle fibers using the potentiometric indicator di-8-ANEPPS. *J. Membr. Biol.* 208:141–153.

17. Woods, C. E., D. Novo, …, J. L. Vergara. 2005. Propagation in the transverse tubular system and voltage dependence of calcium release in normal and mdx mouse muscle fibres. *J. Physiol.* 568:867–880.

18. Cseresnyés, Z., and M. F. Schneider. 2004. Peripheral hot spots for local Ca2+ release after single action potentials in sympathetic ganglion neurons. *Biophys. J.* 86:163–181.

19. Pratt, S. J. P., S. B. Shah, …, R. M. Lovering. 2013. Effects of in vivo injury on the neuromuscular junction in healthy and dystrophic muscles. *J. Physiol.* 591:559–570.

20. Pratt, S. J. P., S. R. Iyer, …, R. M. Lovering. 2018. Imaging analysis of the neuromuscular junction in dystrophic muscle. *Methods Mol. Biol.* 1687:57–72.

21. Pratt, S. J. P., A. P. Valencia, …, R. M. Lovering. 2015. Pre- and post-synaptic changes in the neuromuscular junction in dystrophic mice. *Front. Physiol.* 6:252.

22. Pratt, S. J. P., S. B. Shah, …, R. M. Lovering. 2015. Recovery of altered neuromuscular junction morphology and muscle function in mdx mice after injury. *Cell. Mol. Life Sci.* 72:153–164.

23. Hernández-Ochoa, E. O., C. Vanegas, …, M. F. Schneider. 2016. Alternating bipolar field stimulation identifies muscle fibers with defective excitability but maintained local Ca(2+) signals and contraction. *Skelet. Muscle.* 6:6.

24. McKenna, M. J., J. Bangsbo, and J. M. Renaud. 2008. Muscle K+, Na+, and Cl disturbances and Na+-K+ pump inactivation: implications for fatigue. *J. Appl. Physiol. (1985).* 104:288–295.

25. Hodgkin, A. L., and P. Horowicz. 1959. The influence of potassium and chloride ions on the membrane potential of single muscle fibres. *J. Physiol.* 148:127–160.

26. Meijer, H. J., B. ter Riet, …, T. Munnik. 2002. KCl activates phospholipase D at two different concentration ranges: distinguishing between hyperosmotic stress and membrane depolarization. *Plant J.* 31:51–59.

27. Cannon, S. C., R. H. Brown, Jr., and D. P. Corey. 1991. A sodium channel defect in hyperkalemic periodic paralysis: potassium-induced failure of inactivation. *Neuron.* 6:619–626.

28. Juel, C. 1988. Muscle action potential propagation velocity changes during activity. *Muscle Nerve.* 11:714–719.

29. Kössler, F., F. Lange, …, G. Küchler. 1991. External potassium and action potential propagation in rat fast and slow twitch muscles. *Gen. Physiol. Biophys.* 10:485–498.

30. DiFranco, M., and J. L. Vergara. 2011. The Na conductance in the sarcolemma and the transverse tubular system membranes of mammalian skeletal muscle fibers. *J. Gen. Physiol.* 138:393–419.

31. Jurkat-Rott, K., M. Fauler, and F. Lehmann-Horn. 2006. Ion channels and ion transporters of the transverse tubular system of skeletal muscle. *J. Muscle Res. Cell Motil.* 27:275–290.

32. Lucas, B., T. Ammar, …, J. M. Renaud. 2014. Contractile abnormalities of mouse muscles expressing hyperkalemic periodic paralysis mutant NaV1.4 channels do not correlate with Na+ influx or channel content. *Physiol. Genomics.* 46:385–397.

33. Riisager, A., R. Duehmke, …, T. H. Pedersen. 2014. Determination of cable parameters in skeletal muscle fibres during repetitive firing of action potentials. *J. Physiol.* 592:4417–4429.

34. Waters, C. W., G. Varuzhanyan, …, A. A. Voss. 2013. Huntington disease skeletal muscle is hyperexcitable owing to chloride and potassium channel dysfunction. *Proc. Natl. Acad. Sci. USA.* 110:9160–9165.

35. Zhang, J., R. M. Davidson, …, L. M. Loew. 1998. Membrane electric properties by combined patch clamp and fluorescence ratio imaging in single neurons. *Biophys. J.* 74:48–53.

36. Blijham, P. J., G. J. Hengstman, …, M. J. Zwarts. 2004. Muscle-fiber conduction velocity and electromyography as diagnostic tools in patients with suspected inflammatory myopathy: a prospective study. *Muscle Nerve.* 29:46–50.

37. Nakajima, S., and A. Gilai. 1980. Radial propagation of muscle action potential along the tubular system examined by potential-sensitive dyes. *J. Gen. Physiol.* 76:751–762.

38. Hakansson, C. H. 1956. Conduction velocity and amplitude of the action potential as related to circumference in the isolated fibre of frog muscle. *Acta Physiol. Scand.* 37:14–34.

39. Manttari, S., T. Traskback, and M. Jarvilehto. 2005. Sodium channel development changes the conduction velocity in skeletal muscle. *Basic Appl. Myol.* 15:23–28.

40. Clausen, T., O. B. Nielsen, …, K. Overgaard. 1998. The Na+,K+ pump and muscle excitability. *Acta Physiol. Scand.* 162:183–190.

41. Block, B. A., T. Imagawa, …, C. Franzini-Armstrong. 1988. Structural evidence for direct interaction between the molecular components of the transverse tubule/sarcoplasmic reticulum junction in skeletal muscle. *J. Cell Biol.* 107:2587–2600.

42. Schneider, M. F. 1994. Control of calcium release in functioning skeletal muscle fibers. *Annu. Rev. Physiol.* 56:463–484.

43. St-Pierre, F., J. D. Marshall, …, M. Z. Lin. 2014. High-fidelity optical reporting of neuronal electrical activity with an ultrafast fluorescent voltage sensor. *Nat. Neurosci.* 17:884–889.

44. Muto, A., M. Ohkura, …, K. Kawakami. 2011. Genetic visualization with an improved GCaMP calcium indicator reveals spatiotemporal activation of the spinal motor neurons in zebrafish. *Proc. Natl. Acad. Sci. USA.* 108:5425–5430.

45. Sgobio, C., D. A. Kupferschmidt, …, D. M. Lovinger. 2014. Optogenetic measurement of presynaptic calcium transients using conditional genetically encoded calcium indicator expression in dopaminergic neurons. *PLoS One.* 9:e111749.

46. Beqollari, D., C. F. Romberg, …, R. A. Bannister. 2016. Progressive impairment of CaV1.1 function in the skeletal muscle of mice expressing a mutant type 1 Cu/Zn superoxide dismutase (G93A) linked to amyotrophic lateral sclerosis. *Skelet. Muscle.* 6:24.

47. Braubach, P., M. Orynbayev, …, W. Melzer. 2014. Altered Ca(2+) signaling in skeletal muscle fibers of the R6/2 mouse, a model of Huntington's disease. *J. Gen. Physiol.* 144:393–413.

48. Mukhamedyarov, M. A., E. M. Volkov, …, A. Palotás. 2014. Impaired electro-genesis in skeletal muscle fibers of transgenic Alzheimer mice. *Neurochem. Int.* 64:24–28.